

Amplitude versus offset analyses of the deep sedimentary structures at the northern flank of the Porcupine Basin, SW of Ireland

T. Schmitz · W. Jokat

Received: 1 January 2004 / Accepted: 6 August 2006
© Springer-Verlag 2006

Abstract This paper represents an attempt of analysing the amplitude versus offset (AVO) behaviour and specific seismic attributes of sedimentary structures from the Porcupine Basin, SW of Ireland. During the last decade, a huge number of carbonate mounds were investigated in this region in water depths of 600–1,000 m, but the genesis and growth of these mounds are still not clearly identified. The aim of this paper is to give a better understanding of the connection between fluid migration pathways in the deeper underground and surface expressions of their fluid expulsions like gas chimneys and pockmarks through which the mounds may generate themselves. The data used in this study to determine boundary conditions for the physical properties of the underlying strata were gathered from the northern flank of the Porcupine Basin, where a huge amount of fluid and/or gas chimneys covers the seabed. Marine seismic reflection data contain information about the elastic properties of the underlying earth, mainly based on the observed variations in the seismic reflection amplitude at different shot–receiver offsets. To extract elastic parameters from the data, inversion techniques were used, which presume that input amplitudes are proportional to reflection coefficients for plane wave reflection. To calibrate the AVO analyses with the existing stratigraphy in the working area we have used the well logs from several bore holes in the region. The results of this study show clearly that the investigated and iden-

tified pockmarks on the seafloor are the surface expression of hydrocarbon seepage in the deeper sedimentary underground.

Keywords AVO analysis · Ireland · Mounds · Hydrocarbon seepage

Introduction

This work is a contribution to the geophysical part of the EU-funded project GEOMound (Geological Controls on Mound Foundation). The aim of GEOMound was to advance knowledge of the distribution and evolution of the sparsely known carbonate mound provinces along the European margins of the North Atlantic.

During the last decade, a number of giant carbonate mounds, up to 300 m high, in water depths of 600–1,000 m were investigated by different scientific teams. Prior to this project, only very limited information existed concerning their size, morphology, correlation with hydrocarbon provinces, fluid migration pathways, connection to deeper fault systems, and the surface expressions of their fluid expulsions like gas chimneys, mud volcanoes and pockmarks. Owing to the availability of high resolution and high quality 3D seismic reflection data from one of the cooperation partners (STATOIL), we concentrated, in this study, on the working area Connemara Field, where no carbonate mounds exist, but a huge amount of clearly identified fluid and/or gas chimneys covers the seabed. We interpreted 3D seismic reflection data to investigate the connection of the surface expressions to deeper seated hydrocarbon resources.

T. Schmitz · W. Jokat (✉)
Alfred Wegener Institute for Polar and Marine Research
(AWI), Am Alten Hafen 26, 27568 Bremerhaven, Germany
e-mail: jokat@awi-bremerhaven.de

We determined boundary conditions for the physical properties of the underlying strata using AVO (amplitude versus offset) analyses in the working area (Connemara Field) on the northern flank of the Porcupine Basin. Possible fluid pathways in the vicinity of the mounds, as well as their relationship to structural controls like faults, are highlighted using the results of these analyses.

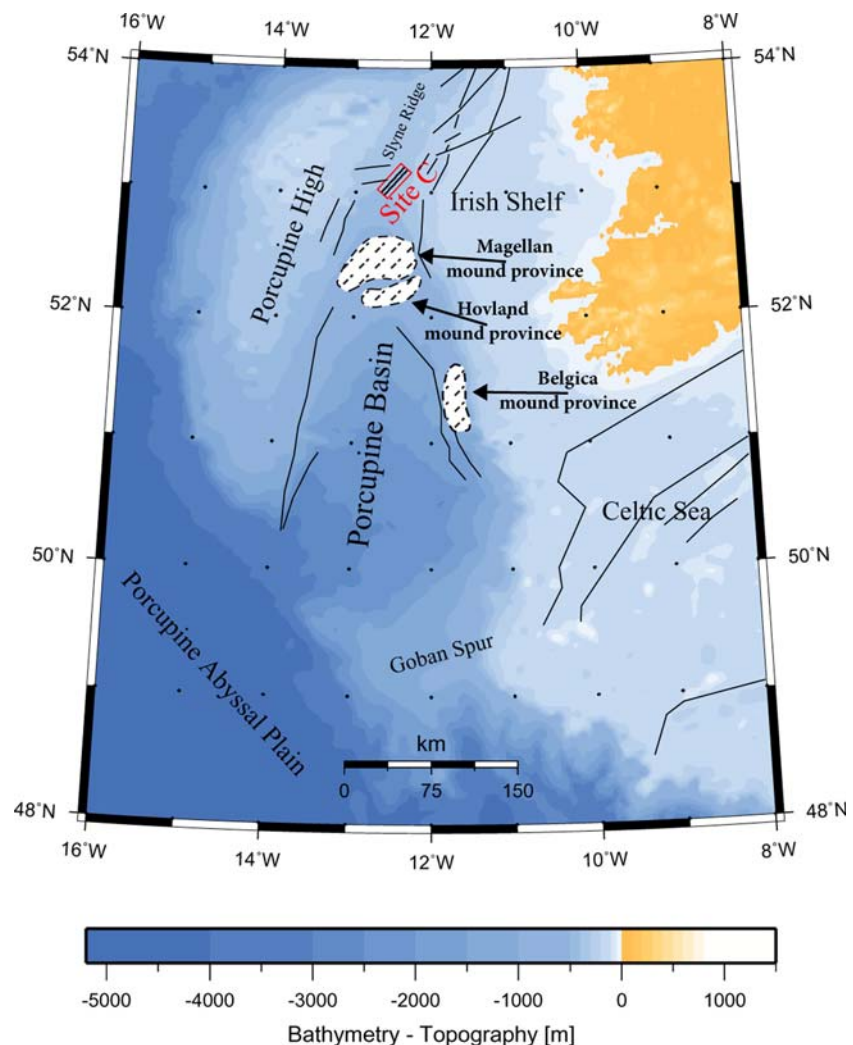
On the basis of five commercial bore holes and their available well logs, Rabaute et al. (2003) did some clustering analyses that provided information on the physical properties of the seismic layers and proposed a seismic stratigraphy in the working area. These results are used to calibrate the AVO analyses.

Study area

The Porcupine Basin (Fig. 1) is a triangular Mesozoic to Cenozoic rift basin on the continental shelf off the

west coast of Ireland. It is orientated approximately North–South, about 230 km long and between 65 and 100 km wide. Water depths vary between 150 m in the north and 3,000 m in the south, where the basin opens into the Porcupine Abyssal Plain. The underlying basin structure is bordered by the Porcupine High (Porcupine Bank) to the west, the Slyne Ridge to the north, the Irish continental Shelf to the east and the Goban Spur to the south (Moore and Shannon 1992). These surrounding platforms consist of Precambrian and Palaeozoic metamorphic rocks, whereas the basin itself is the result of a failed rift event in the proto-North Atlantic. The basin contains up to 10 km of sediments that were deposited mainly during the Mesozoic and Cenozoic post-rift period, and thin northwards and towards the flanks of the basin (Van Rooij et al. 2003). The basin developed in parallel during two major rifting periods, in the Permo-Triassic and the Middle to Late Jurassic. Hydrocarbon reservoirs of Jurassic and Cretaceous ages were discovered during the drilling of

Fig. 1 Bathymetry of the Porcupine Basin and its surrounding platforms, and location of the working area at the GEOMound working Site C. The faults are taken from Naylor and Shannon (1982) and Ziegler (1982). The mound provinces in the Porcupine Basin are taken from Huvenne et al. (2003)



some wells in the northern parts of the basin (Moore and Shannon 1992).

Geology of the study area

The Connemara Field is located at the northern flank of the Porcupine Basin (Fig. 1) and is structurally mainly influenced by the conjunction of two principal fault systems. A North–South striking fault regime which represents the main orientation of the basin itself, and a combination of East–West and Northeast–Southwest trends which appear to be reactivated Caledonian faults (Rabaute et al. 2003). The Connemara Field appears as a heavily faulted, tilted block structure with a general southwestern dip, and is bordered by major faults to the east and west. Some synclinal southwest basins with their axes parallel to the major faults are filled with Mesozoic sediments (Rabaute et al. 2003). Most of the Mesozoic sediments lie unconformably on Paleozoic rocks. Dense coverage of 2D and 3D seismic lines in the Connemara Field shows numerous diffuse vertical zones, which indicate vertical fluid and/or gas pathways. These pathways are mainly concentrated above structural highs. Hydrocarbons in the Connemara Field are likely to have originated and matured in Jurassic source rock in the Southern Porcupine Basin, followed by up-dip (northwards) migration to Jurassic traps or to the surface through fault planes or other tectonic unconformities (Rabaute et al. 2003). Rabaute et al. (2003) interpreted more than 1,100 pockmarks in 2D seismic data in the Connemara Field which had been formed through the escape of methane at the seafloor and could be a surface expression of hydrocarbon seepage. To date, no exposed or buried carbonate mound structures are known in the Connemara Field area.

Methods and data

Data

A total of 230 km of 2D seismic data and 380 km² of 3D seismic data were acquired between July and September of 1996 by the seismic contractor Geco (Seisquest) for STATOIL. The working area (Fig. 1) is part of the Connemara Oil Field and is named “Site C” in the GEOMound project description, between 52°57′N to 53°15′N and 12°42′W to 12°15′W.

Two airgun arrays, each with two 43.1 l G-Guns, were used as seismic source. The shot interval was 18.75 m. Four SYNTRAC streamers with a total of 1,152 channels and a group interval of 12.5 m recorded

the data in SEG-D format with a sampling interval of 4 ms. The line spacing, controlled by GPS, was 12.5 m and the total length of each profile was about 30.5 km. To get a proper fold for CDP sorting of each profile, the adjacent profiles overlapped by 25 m (Fig. 2). The data quality reported by Geco was “fair”. The dominant frequency of the data sets was determined by a spectral analysis tool to be around 38 Hz, with an averaging bandwidth of 20 Hz.

It was not possible to calculate a complete 3D AVO analyses set within this project, due to time-consuming computations for each AVO analysis. Typical results for the AVO analyses are shown on profile GEO01169 for the north-western area of the Connemara Field and on profile GEO01313 for the south-eastern area.

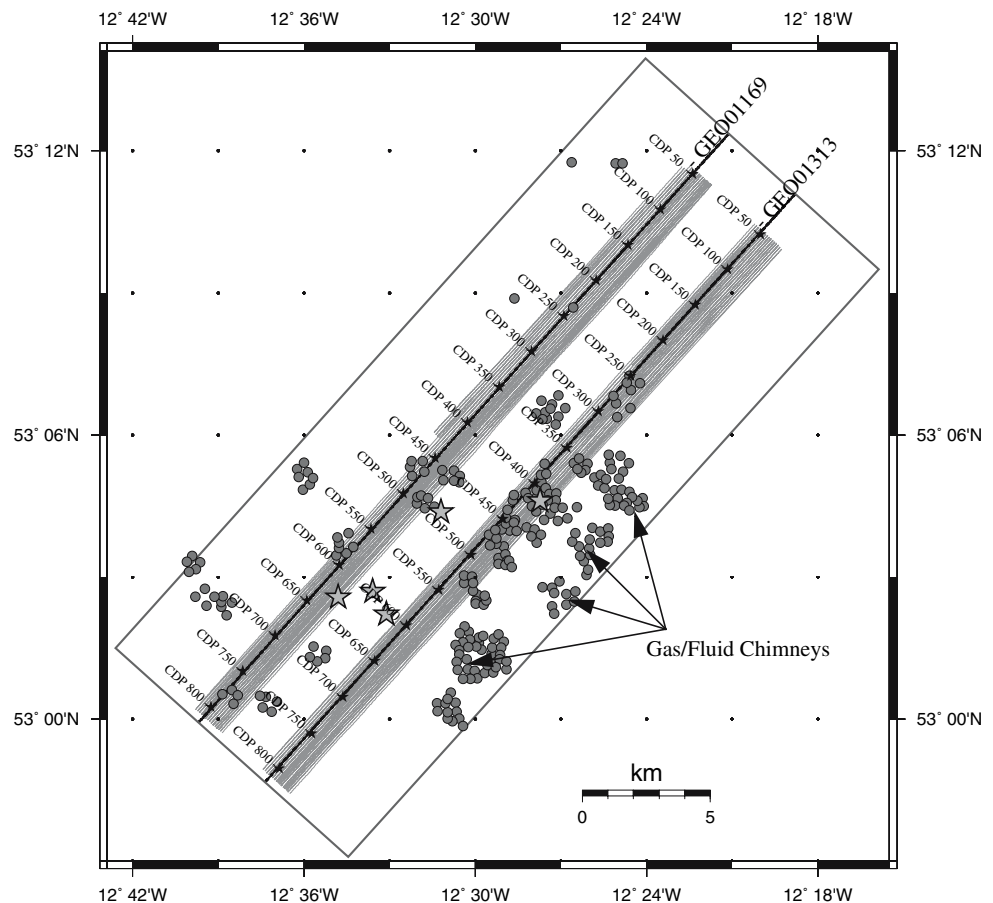
In addition to the unstacked CDP-gathers, STATOIL has made available a smoothed Interval-Migration-velocity file from a 3D-velocity cube. The file contains 60 pairs of depth/velocity values from 0.0 to 5.4 s TWT (Two-Way-Traveltime) for each inline/crossline cross-over point. In total, the 3D seismic block (ST 9605) contains 25 inlines and 63 crosslines, which results in 1,575 cross-over points with a spacing of 12.5 m in both the inline and crossline directions. This study uses a subset of 15 inlines divided up into two blocks (Fig. 2) to image the deeper structure beneath the surface expulsion structures. Sixty different cross sections were calculated over the entire 3D area, each for one discrete depth, to display the spatial distribution of the velocity variations. The visual interpretation of these slices shows a very uniform velocity distribution with small lateral variations at depths of 1.0–1.7 s TWT. Velocity models were calculated along each seismic profile as an input for the AVO software based on these grid slices.

Principles of AVO analysis

The amplitude of a plane wave reflection depends on the material contrast across the reflecting interface ($\Delta V_P/V_P$, $\Delta V_S/V_S$, $\Delta\rho/\rho$) and its incident angle at the interface. This angle dependency allows, in theory, the values of $\Delta V_P/V_P$, $\Delta V_S/V_S$ and $\Delta\rho/\rho$ to be calculated, thereby providing a tool to estimate layer composition and fluid saturation directly from the data. In practice, kinematic, dynamic and experimental factors limit the resolution of these parameters.

The Zoeppritz equation describes the relationship between the amplitudes of reflected and transmitted compressional- (P) and shear- (S) waves across an interface, in terms of their incidence. The Zoeppritz equation can be simplified by making some approximations that describe the variation of P -wave reflection coefficients with the angle of incidence as a

Fig. 2 CDP-gathers of all 15 processed profiles (in grey) and the position of the two stacked profile lines (GEO01169 and GEO01313) that are presented in this paper. Each profile consists of four streamers and adjacent profiles overlapping by 25 m, which means that the third and fourth streamer of the first profile has the same position as the first and second streamer of the second profile. The dark grey circles/dots represent gas and/or fluid chimneys identified by STATOIL along 2D seismic lines. The stars show the position of five commercial bore-holes



function of the P -wave velocity, the S -wave velocity and the densities above and below the interface (Smith and Gidlow 1987).

In this study, two approximations for the Zoeppritz equation were used for the AVO analyses. Shuey (1985) reduces the Zoeppritz equation for all angles of incidence to two terms:

$$R(\Theta) = A + B \sin^2 \Theta + \dots,$$

where R = reflection coefficient; θ = angle of incidence; A = AVO intercept; B = AVO gradient.

This approximation represents the angular dependence of P -wave reflection coefficients using two parameters: the AVO intercept (A) and the AVO gradient (B). In practice, the AVO intercept (A) is a band-limited measure of the normal incidence amplitude, while the AVO gradient (B) is a measure of amplitude variations with offset. Assuming appropriate amplitude calibration, A is the normal incidence reflection coefficient and B is a measure of offset dependent reflectivity (Castagna 1997). Hydrocarbon related AVO anomalies may show increasing or decreasing amplitude variations with offset due to the presence of fluid and/or gas. AVO

interpretation is facilitated by crossplotting the AVO intercept against the AVO gradient. Under normal geological circumstances, the intercepts and gradients for “background” rocks follow a well-defined background linear trend in the crossplot. AVO anomalies are properly viewed as deviations from this background and may be related to hydrocarbon or lithologic factors depending on in which part of the crossplot they appear (Castagna 1997).

Amplitude versus offset inversions using the Shuey approximation obtain the following attribute sections: The Normal Incidence Reflectivity section (A) and the AVO gradient section (B). For small angles of incidence, B is the rate of change of amplitude with respect to offset. Although this relationship is a poorer approximation of the Zoeppritz equation, it is often sufficient to delineate areas of anomalous AVO behaviour.

For a conventional stacked trace, the amplitude value for a given time is the average of the amplitudes over all offsets. Using this average does not consider the relative amplitude changes encoded in the offset distribution. However, for a normal incidence trace, AVO data, which gives the amplitude value depending on the offset, are used to compute the normal inci-

dence amplitude. A normal incidence section can therefore be considered as a better zero-offset section than a conventional stack section.

In Shuey’s formula, the coefficient B is directly related to elastic parameters. It can be shown that a strong variation in the V_S/V_P ratio across the interface produces a high absolute value of B . Since gas in porous rocks greatly affects the V_S/V_P ratio (Ostrander and Gassaway 1983), gradient sections are often good indicators of gas reservoirs.

The second approximation of the Zoeppritz equation is that of Aki and Richards (1979), which makes the following assumptions for the seismic reflection data: firstly, the relative change of the rock properties $\Delta V_P/V_P$, $\Delta V_S/V_S$ and $\Delta \rho/\rho$ are sufficiently small so that second-order terms of the Zoeppritz equation can be neglected and, secondly, θ does not approach the critical angle or 90° . The approximated Zoeppritz equation thus reads

$$R(\Theta) = \frac{1}{2} \left(1 - 4 \frac{V_S^2}{V_P^2} \sin^2 \Theta \right) \frac{\Delta \rho}{\rho} + \frac{1}{2 \cos^2 \Theta} \frac{\Delta V_P}{V_P} - 4 \frac{V_S^2}{V_P^2} \sin^2 \Theta \frac{\Delta V_S}{V_S},$$

where R = reflection coefficient; V_P = average P -wave velocity; V_S = average S -wave velocity; ρ = average density; θ = average of angles of incidence and transmission.

Amplitude versus offset inversions using the Aki and Richards linearised approximation of the Zoeppritz equation yield the following attribute sections: P -wave reflectivity section ($\Delta V_P/V_P$), S -wave reflectivity section ($\Delta V_S/V_S$), as a lithology indicator of their linear combinations being the pseudo Poisson reflectivity ($\Delta \theta/\theta = \Delta V_P/V_P - \Delta V_S/V_S$), and the Fluid Factor. The Fluid Factor, a hydrocarbon indicator, is a deviation from the “mudrock line” of Castagna et al. (1985) that gives a relation of P -wave velocity to S -wave velocity for water-saturated clastic silicate rocks. The Fluid Factor is given as

$$F = \frac{\Delta V_P}{V_P} - \beta \left(\frac{V_S}{V_P} \frac{\Delta V_S}{V_S} \right)$$

for which β is defined by the Mudrock Line formula (Castagna 1997) and is by default set at 0.86.

For water-saturated clastic silicates, the Fluid Factor should be zero everywhere except where gas has displaced part of the water. On the basis of in situ sonic and field measurements done by Castagna et al. (1985), we estimated the V_P/V_S ratio for mudrocks in the Connemara Field to be

$$V_S = 0.86V_P - 1,360 \left[\frac{m}{s} \right]$$

Data processing

The AVO inversion used by the PARADIGM Probe software is essentially a weighted stack process, so that the data must be corrected for moveout. For an almost 1D earth, the hyperbolic moveout approximation gives stacking results that constitute a good input to the inversion. The implementation of AVO attribute analysis is performed across iso-time sample values. Input gathers are assumed to be moveout corrected. Multiple energy, and other forms of coherent and random noise, degrade the AVO analysis and should be eliminated beforehand. The problems caused by noise can be reduced by the input of supergathers consisting of three CDPs and the application of a median filter (Paradigm Geophysical).

The pre-processed STATOIL data sets (CDP-gathers as well as velocity files) were converted into the international SEG-Y format and loaded into the AVO-Inversion software package.

We used the basic inversion workflow described below (Fig. 3) for the analyses of the original unstacked CDP-gathers.

1D-raytracing is first performed on the data based on the available smooth background interval velocity model and assuming horizontal or only gently dipping

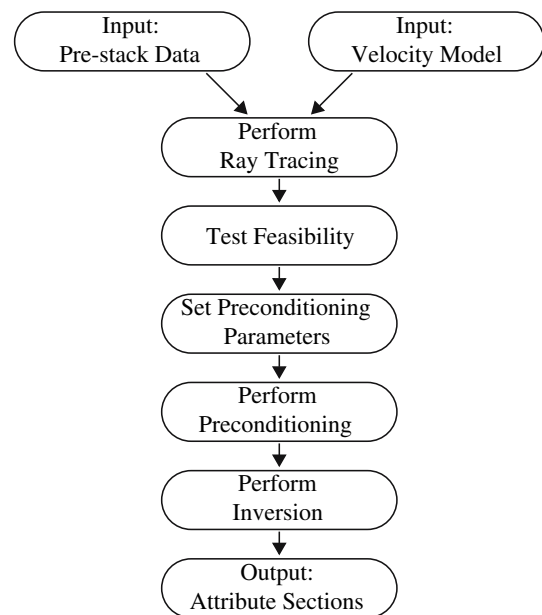
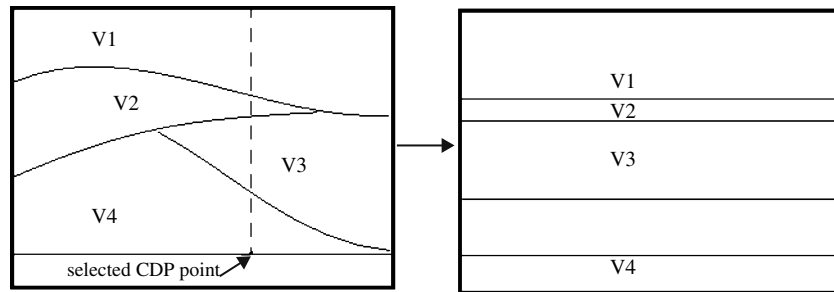


Fig. 3 Basic workflow for the AVO inversion using the PARADIGM Probe software

Fig. 4 At a given CDP location, a 1D velocity model is extracted. 1D-raytracing is performed using this local velocity model



strata. 1D-raytracing calculates the ray information for each point in the stacked section and transfers the travel time information to a layer model, depending on the background velocity from the interval velocity model (Fig. 4).

The raytracing output provides information about the angle of entrance at the source, the angle of emergence at the receiver, the angle of incidence at all interfaces, and the ray path length. This information is used to perform AVO pre-conditioning and inversion. The angle of incidence can be found as a function of time and offset by iterative ray tracing. In particular, the angle of incidence can be computed for each sample in a normal moveout corrected CDP-gather (Smith and Gidlow 1987).

Ray tracing information is used in the inversion work flow at two stages. The first stage is pre-conditioning. Corrections such as source array response and source directivity require information on the angle of entrance. Receiver array response and receiver directivity requires information about the angle of emer-

gence. Geometrical spreading corrections are calculated dynamically by the raytracing, and the Q (Quality) factor attenuation requires information about the ray path. The second stage is inversion. AVO inversion is based on an approximation of the Zoeppritz equation, which relates reflection coefficients to the angle of incidence. Therefore, the angle of incidence at every time/offset sample is required. The more accurate the angle of incidence is calculated, the more reliable the results of inversion will be. The Shuey approximation of the Zoeppritz equation can be fitted to the amplitudes of all traces at each time sample of the CDP-gather, and certain rock properties can be estimated.

It is useful to perform an “AVO feasibility test”, which estimates the feasibility of inversion prior to the AVO analysis processing. The inversion algorithm calculates an internal matrix that contains the results of the test. By evaluating the properties of this matrix before performing the inversion, it is possible to estimate the stability of the inversion process. During this

Fig. 5 Graphical delineation of the Probe AVO Inversion feasibility test for the Shuey approximation inversion type. The upper part shows the complete section GEO01169 and the lower one only the first 1,500 ms

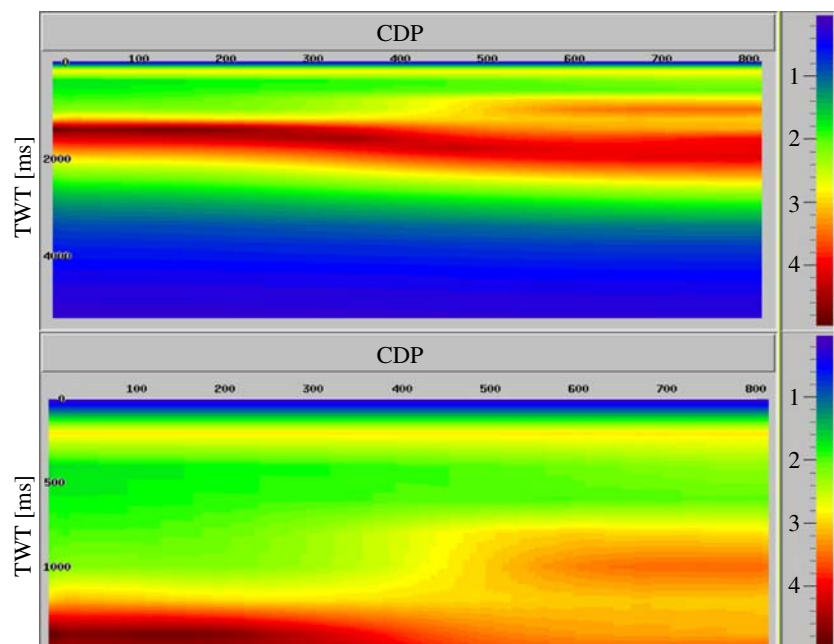
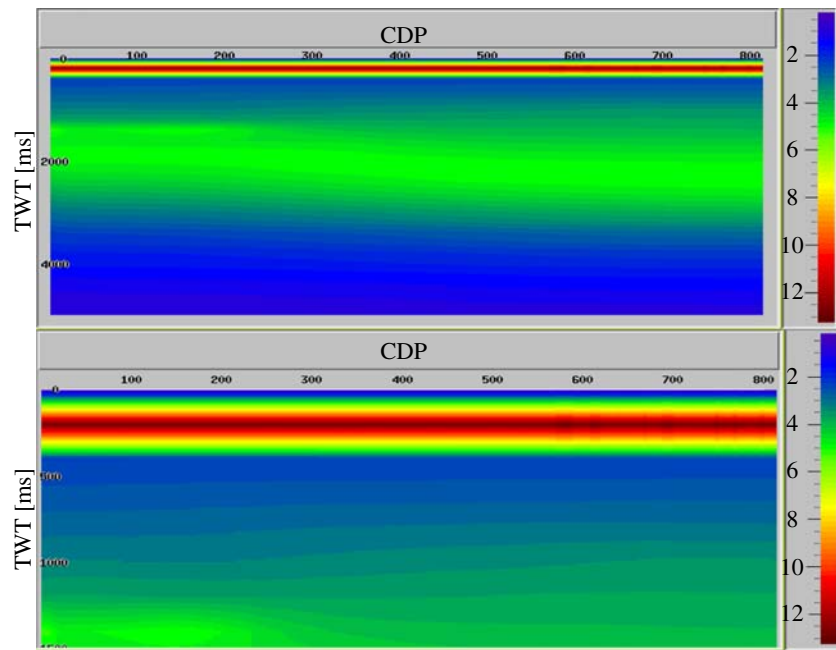


Fig. 6 Graphical delineation of the Probe AVO Inversion feasibility test for the Aki and Richards approximation inversion type. The *upper part* shows the complete section GEO01169 and the *lower one* only the first 1,500 ms



feasibility test, a feasibility value starting with 0 is assigned to each point on the section (Figs. 5, 6). The “AVO feasibility test” performed by the Probe software package considers any value above 0.3 to be feasible; however, the higher the value, the more stable the inversion. The results are not feasible for example, if the angle range is small or if the angles are irregularly distributed within the given range.

To extract the elastic parameters of the underlying earth from the marine seismic reflection data, the Probe software uses inversion techniques presuming that input amplitudes are proportional to reflection coefficients for plane wave reflection. Consequently, other amplitude scaling effects must be removed from the data. During our processing sequence, the following amplitude scaling effects were removed:

- Absorption (Q-correction), which is the attenuation caused by non-elastic absorption during wave propagation
- Source directivity, which corrects for the directionality of individual source elements
- Receiver directivity, which corrects for the directionality of individual receiver element to account for ghost interference effects
- Geometrical spreading, which is caused by wave front energy dissipation.

A median filter with a length of 3% of the maximum offset range is used to increase the signal/noise ratio in the offset direction and to remove interference by multiples.

Q factor attenuation is generally approximated by an exponential decay, which depends primarily on the Q factor and the length of the travel time path. Assuming that the frequency-dependent nature of the problem can be exchanged with a centre frequency approximation, a single correction for each (t, x) point can be calculated. We can calculate the difference between the true travel path and the zero offset travel path for all samples on the moveout corrected gather with an assumed average effective Q factor of 100, (for moderate to high attenuation) and the background velocity model. Each sample is then corrected accordingly. Many of the pre-conditioning corrections to be applied are frequency dependent.

The next important step in the processing flow is the application of amplitude-preserving pre-stack migration before performing the AVO inversion. Migration causes the diffractions to collapse and narrows the Fresnel zone, making the results of AVO inversion more accurate. The amplitude-preserving pre-stack depth migration is done using an FX migration algorithm that is applied to the 2D attribute sections. The selected and above-described pre-conditioning functions are applied and the NMO (normal move out) corrected data are sorted into common offset sections. A zero-offset FX depth migration is applied to each offset plane and the migrated offset sections are sorted into CRP (common reflection point) depth gathers. Then the depth gathers are scaled to the time migrated domain. The FX algorithm used by the Probe software is described by Soubaras (1996).

Ultimately, we can analyse the measured amplitude variations as a function of incident angle and obtain attribute sections that measure various elastic parameters after applying proper model-based pre-conditioning to the data and 1D-raytracing through the background velocity model to obtain the angles of incidence for all desired reflectors.

Results

During this work, AVO analyses were carried out for a total of 15 profiles shown in Fig. 2. Example interpretations of the AVO results are shown for profiles GEO01169 in the north-western Connemara Field, and GEO01313 in the south-eastern area. The results of these AVO analyses are supported by the results of AVO analyses done at the other lines shown in Fig. 2.

The results of the sensitivity tests for both approximation inversion types for profile GEO01169 (Figs. 5, 6) show a proper feasibility and consequently a stable inversion for the AVO analyses for most of the travel times. For the Shuey approximation, a feasibility value greater than 0.3 is achieved from 30 ms down to 4,800 ms (Fig. 5). For the Aki and Richards approximation, proper values are from 60 ms down to 5,000 ms (Fig. 6). With an average water depth of 220 m (=300 ms TWT), the results of both approximation inversion types are stable for the complete seismic section. The results are similar for the profile GEO01313, so that reasonable AVO analyses were performed for both profiles.

Borehole results, reported by BP from four sites less than 2 km away from profiles GEO01169 and GEO01313 (Fig. 2), allow the seismic stratigraphy to be interpreted as geological units. Figures 7 and 8 show the normal stacked sections of profiles GEO01169 and GEO01313 as well as the stratigraphic interpretation and geological ages of the layers. The two sections show that the deeper sedimentary structures are strongly affected by tectonism. The age of the sediments range from at least Middle Jurassic to Tertiary.

The AVO analyses provide additional constraints and the results of the different approximations are shown in Figs. 8, 9, 10, 11, 12, 13 and 14.

Zones of low amplitude or diffuse reflections appear in the stacked sections of profiles GEO01169 and GEO01313 (Figs. 7, 8) but could be seen much better in the AVO analysed sections (Figs. 10, 11, 13, 14) and might be interpreted as evidence for fluid and/or gas chimneys or pathways through the sediments. These zones are concentrated in the upper part (500–1,200 ms TWT) of profile GEO01169 (Fig. 7) between CDPs 400 and 470 and between CDPs 550 and 680. On profile GEO01313 (Fig. 8), the zones of low amplitude are concentrated between CDPs 250 and 300 and between CDPs 400 and 480. Low amplitude zones correlate with the edge of an anti-clinal uplift of the stratigraphy that is prominent on both profiles (Figs. 7, 8).

The visualisation of the measured amplitude variations, as a function of incidence angle, is shown in the weighted stacking results for profile GEO01169 (Fig. 9) using the Aki and Richards approximation to the Zoeppritz equation. All four panels show the same

Fig. 7 Stacked section and stratigraphy of profile GEO01169. LAZ low amplitude zones

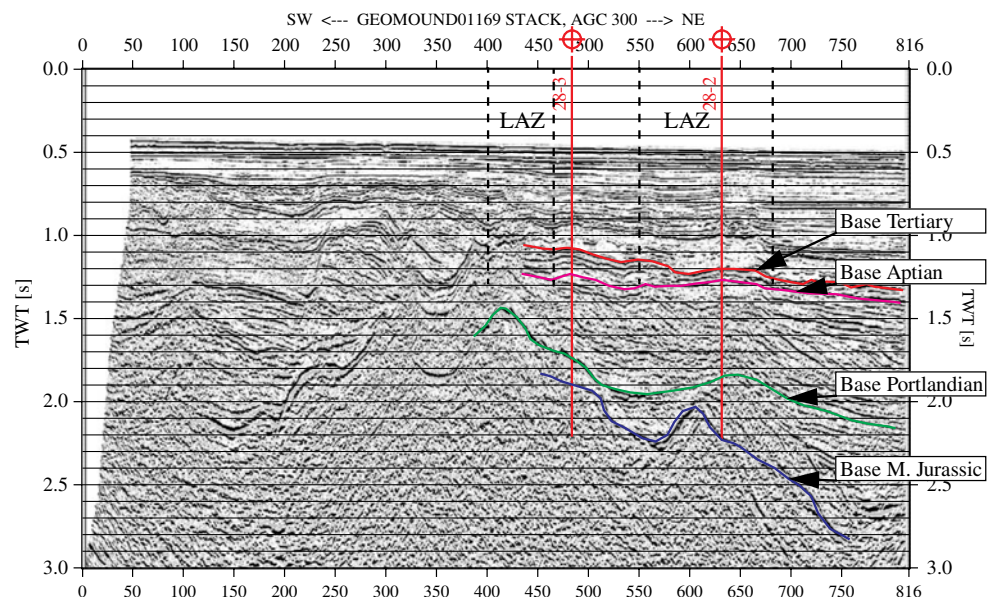


Fig. 8 Stacked section and stratigraphy of profile GEO01313. LAZ low amplitude zones

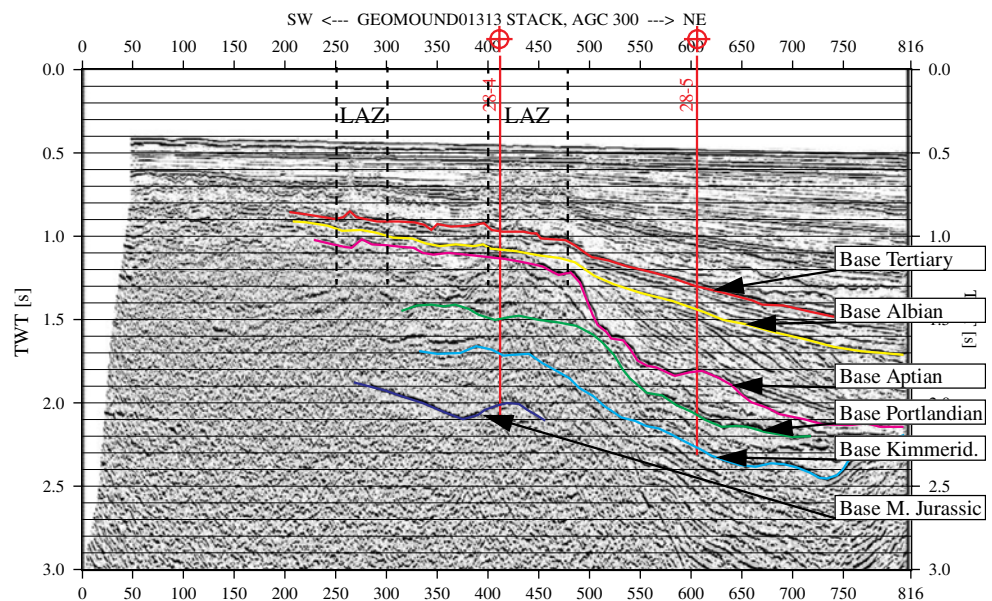
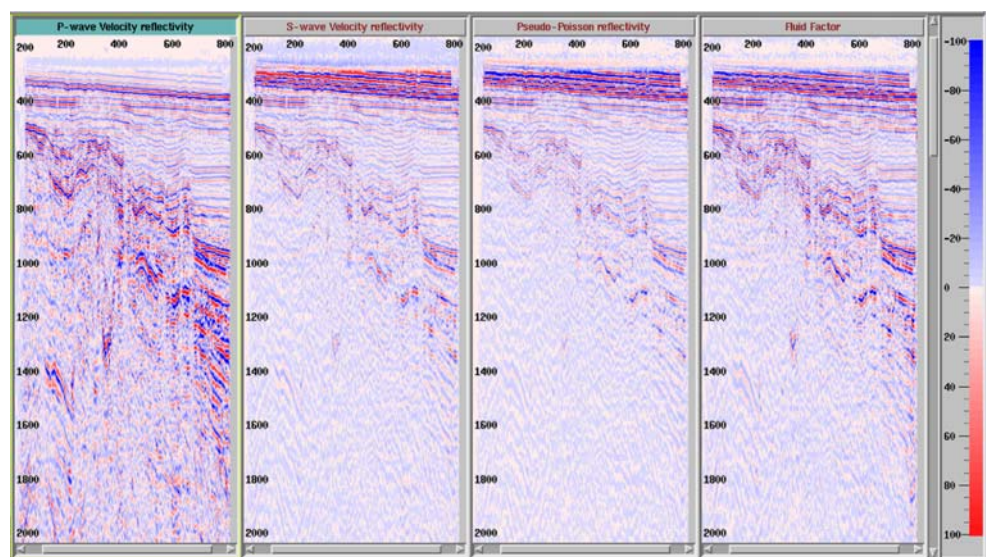


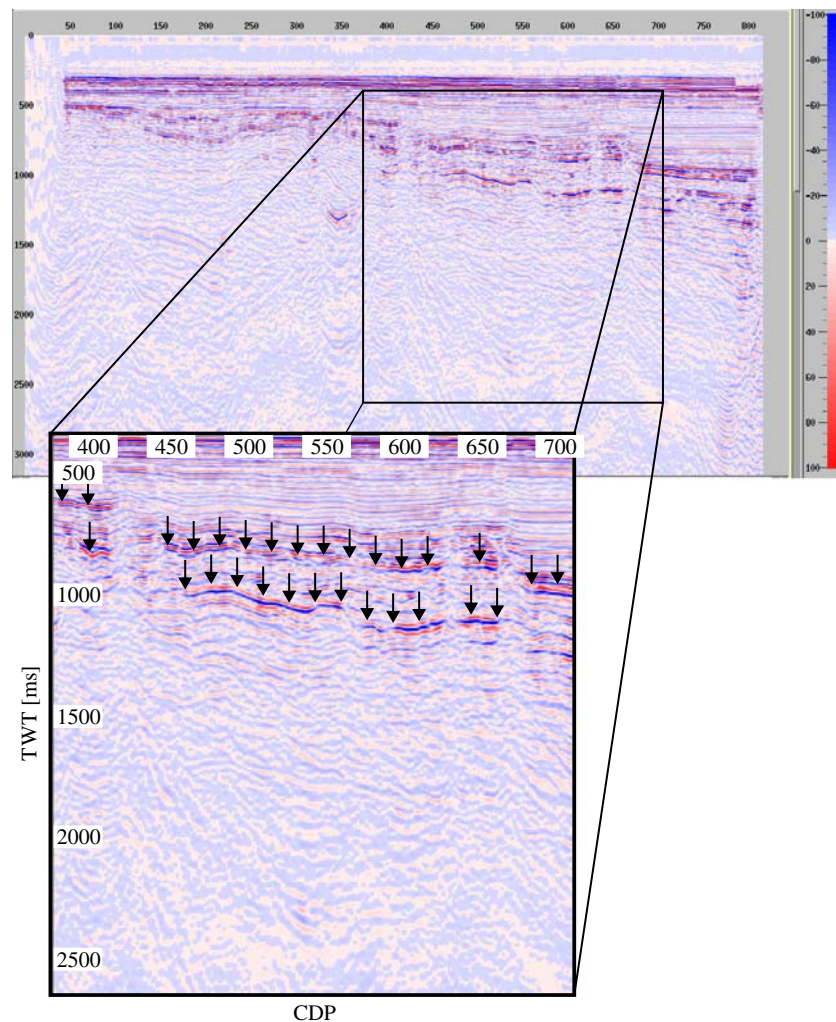
Fig. 9 Inversion results using the Aki and Richards approximation to the Zoeppritz equation for profile GEO01169. Sections from left to right: *P*-wave velocity reflectivity, *S*-wave velocity reflectivity, pseudo-Poisson reflectivity and Fluid Factor. All sections are displayed without any post-stack processing except a uniform post-stack gain curve to balance the appearance of the sections. For this reason, the amplitudes of the various reflectivities are comparable from one display to another



amplitude-dependent section. The *S*-wave velocity section is calculated with the formula of Castagna et al. (1985). The pseudo-Poisson reflectivity shows the normalised change in pseudo-Poisson ratio. For water-saturated clastic silicates, the Fluid Factor as well as the pseudo-Poisson reflectivity should be zero over the complete profile. The AVO analyses show that this is not the case. The Fluid Factor along both profiles GEO01169 (Fig. 10) and GEO01313 (Fig. 13) has a non-zero value over different regions (marked with arrows). This result provides strong evidence that, in these regions, gas has displaced the water or at least residuals of percolated gas are present in the layers.

On the basis of Shuey’s two-term approximation, the AVO analyses provide two inversion results: Normal Incidence Reflectivity and AVO Gradient. The Normal Incidence Reflectivity section for profile GEO01169 (Fig. 11) also shows some anomalous gaps, especially along and above the Base Tertiary reflector (marked red in Fig. 7). Normal Incidence Reflectivity and AVO gradient are plotted against each other to facilitate the AVO interpretation. The crossplots (Figs. 12, 15) show a linear trend (the Mud Rock Line, after Castagna et al. 1985) on both profiles GEO01169 and GEO01313. Additionally, a distinct deviation from this background trend can be observed in both cross-

Fig. 10 Weighted stacked section of profile GEO01169 showing the Fluid Factor based on the Aki and Richards approximation to the Zoeppritz equation. *Arrows* mark the reflectors with unusually high amplitudes. For water-saturated clastic silicates, the Fluid Factor should be zero over the complete profile



plots as well. Crossplotting can only give a conclusion for the entire profile because it does not work with single layers but only with complete sections. These results are either interpreted as the result of distinct lithological changes over the entire profile, or may highlight the fluid/gas content of some of the layers.

Discussion

The uplift structure in both profiles GEO01169 and GEO01313 (Figs. 7, 8) is interpreted as occurring over a basement high, which is represented by the acoustic basement in the area. Hydrocarbon reservoirs, based on the well-log analyses, are potentially located in the Kimmeridgian and Portlandian. In the north-western part of the working area, gas and/or fluid chimneys, identified by STATOIL along 2D seismic lines, are scarce while in the south-eastern area gas chimneys are numerous (Fig. 2).

We find striking correlations if we combine the AVO results of line GEO01169 (Figs. 10, 11) with the information on the location of gas chimneys at the sea floor (Fig. 2) and the geological interpretation. Some clustering of chimneys occurs between CDPs 450 and 550 of line GEO01169 (Fig. 2) in a zone almost 2 km wide. In the deeper part of the seismic section at almost 1 s TWT (Fig. 7), the Base Tertiary reflector with varying AVO parameters is observed (Figs. 10, 11). These variations are interpreted to represent clastic silicate rocks, like porous sandstone, whose water content has been partly replaced by gas. By means of lithological analyses of drilled samples from the adjacent boreholes, Rabaute et al. (2003) show that the Base Tertiary layers consists of partially lithified sand and sandstone, which supports the interpretation of the AVO results.

Three smaller portions of this reflector, at CDPs 570, 630 and 660, show low values in the Fluid Factor panel (Fig. 10) and Normal Incidence plots (Fig. 11). Smaller

Fig. 11 Normal Incidence Reflectivity section based on the Shuey approximation to the Zoeppritz equation for profile GEO01169. The *black marked* reflector is the Base Tertiary boundary. *Arrows* mark the diffuse regions with unusually low amplitudes

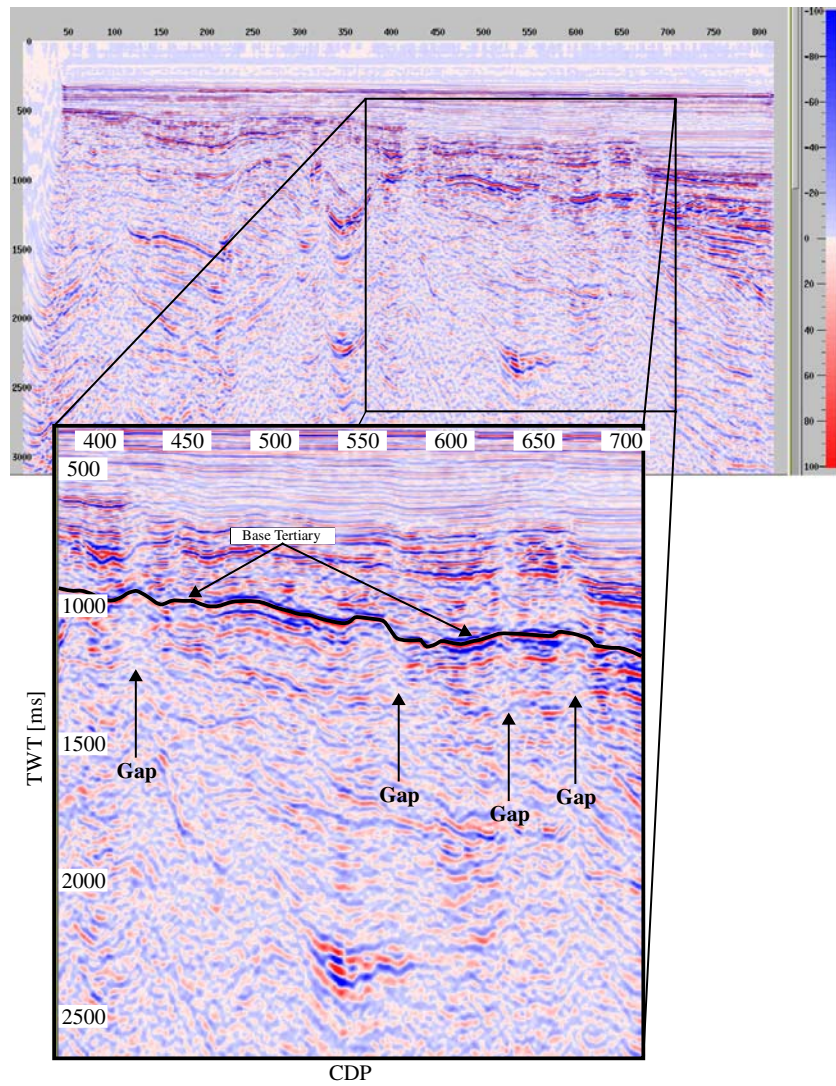
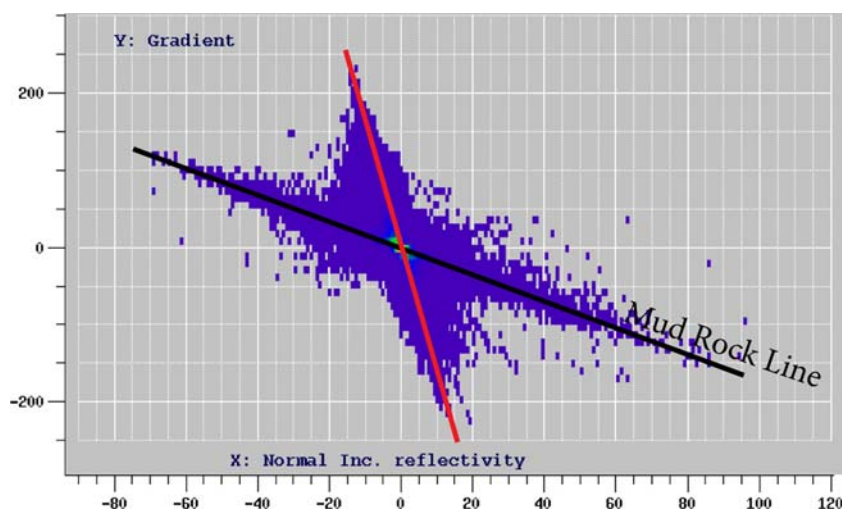


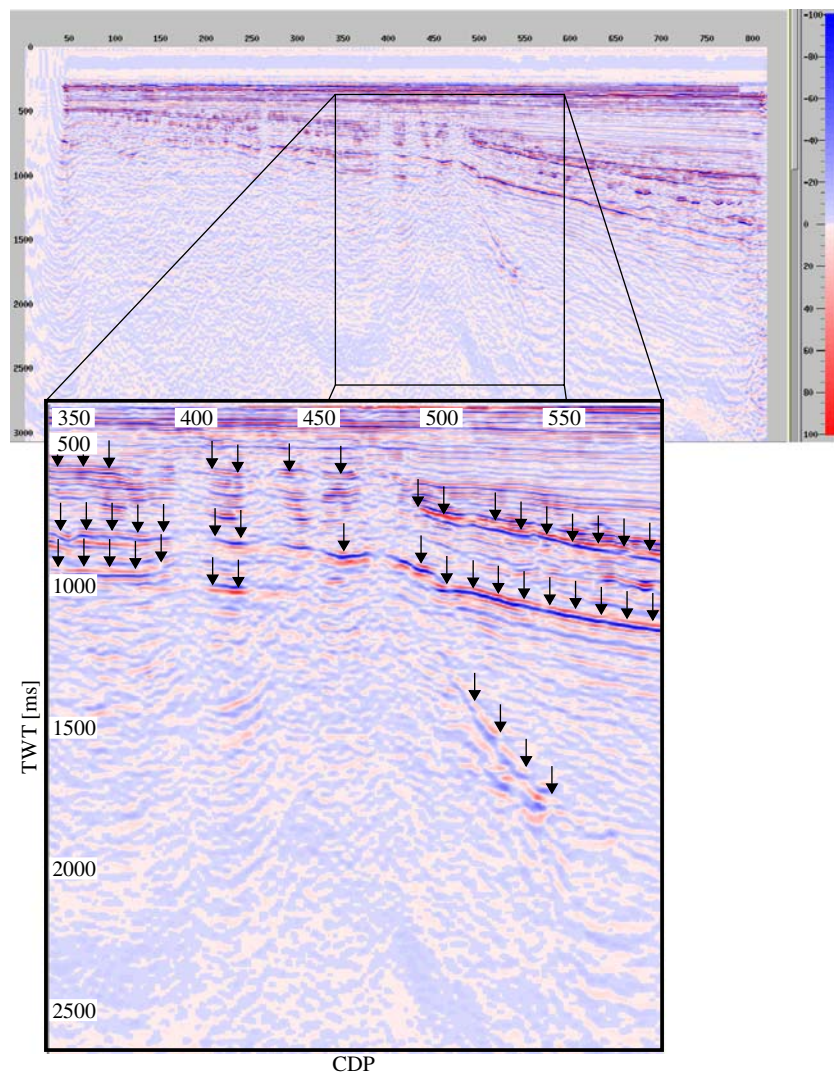
Fig. 12 Crossplot of normal incidence reflectivity against AVO gradient for profile GEO01169. The *black line* represents the linear background trend (which is a typical one for clastic silicate rocks) and the *red line* the AVO anomalies over the complete profile which are properly viewed as deviations from the background trend and may be related to hydrocarbons in the underground



gas chimneys were mapped in the vicinity of these deep-seated variations in the layer lithology. Low seismic amplitudes occur and almost reach the sea floor

in between these anomalous zones. These results give strong evidence for the percolation of gas and/or oil through the Tertiary sediments. The hydrocarbons

Fig. 13 Weighted stacked section of profile GEO01313 showing the Fluid Factor based on the Aki and Richards approximation to the Zoeppritz equation. Arrows mark the reflectors with unusually high amplitudes. For water-saturated clastic silicates, the Fluid Factor should be zero over the complete profile



could have reached the sea floor in the areas where gas chimneys occur. We suspect that for the shallow part of the seismic section the resolution of the data is not good enough to image these small-scale features or older chimneys. Rabaute et al. (2003) report that most of the chimneys terminate at the Plio-Pleistocene boundary and do not reach the present sea floor surface.

The situation is slightly different for the more southerly profile GEO01313 (Fig. 8) and (Figs. 13, 14, 15). Here, a significantly larger number of gas chimneys were mapped by STATOIL between CDPs 380 and 480 (Fig. 2). The gas pathways in the subsurface are closely related to the basement high or anti-clinal uplift of Middle Jurassic age between CDPs 400 and 500. The structure might be a rotated block, formed during the Jurassic rift phases. Some reflectors, like the Middle Jurassic one, are clearly displaced above this structural high (Fig. 8). This may be due to differential

compaction on either side of the high, or to a reactivation of old fault zones. In the latter case, these fault zones might have allowed the migration of gas and/or oil to the sea floor. By means of lithological analyses of the drilled samples, Rabaute et al. (2003) indicate that the potential source area seems to be of Middle or Upper Jurassic age (Kimmeridgian to Portlandian) and consists of sandstones. The Kimmeridgian and Portlandian appear as gently dipping reflectors at 1,500 ms TWT (Fig. 8, CDP 500) in the hanging wall of the fault bounding the basement high. Here, the AVO panels for the Fluid Factor (Fig. 13) and the Normal Incidence Reflectivity (Fig. 14) show clear variations. The high amplitudes around CDP 500 at about 1,500 ms TWT indicate that gas concentrations might be present close to the fault. The Kimmeridgian to Portlandian layers have a different appearance over the basement uplift (CDPs 350 to 450, Fig. 12). The AVO parameters show lower amplitude values where the layers are

Fig. 14 Normal Incidence Reflectivity section based on the Shuey approximation to the Zoeppritz equation for profile GEO01313. The *black* marked reflector is the Base Portlandian boundary. *Arrows* mark the diffuse regions with unusually low amplitudes

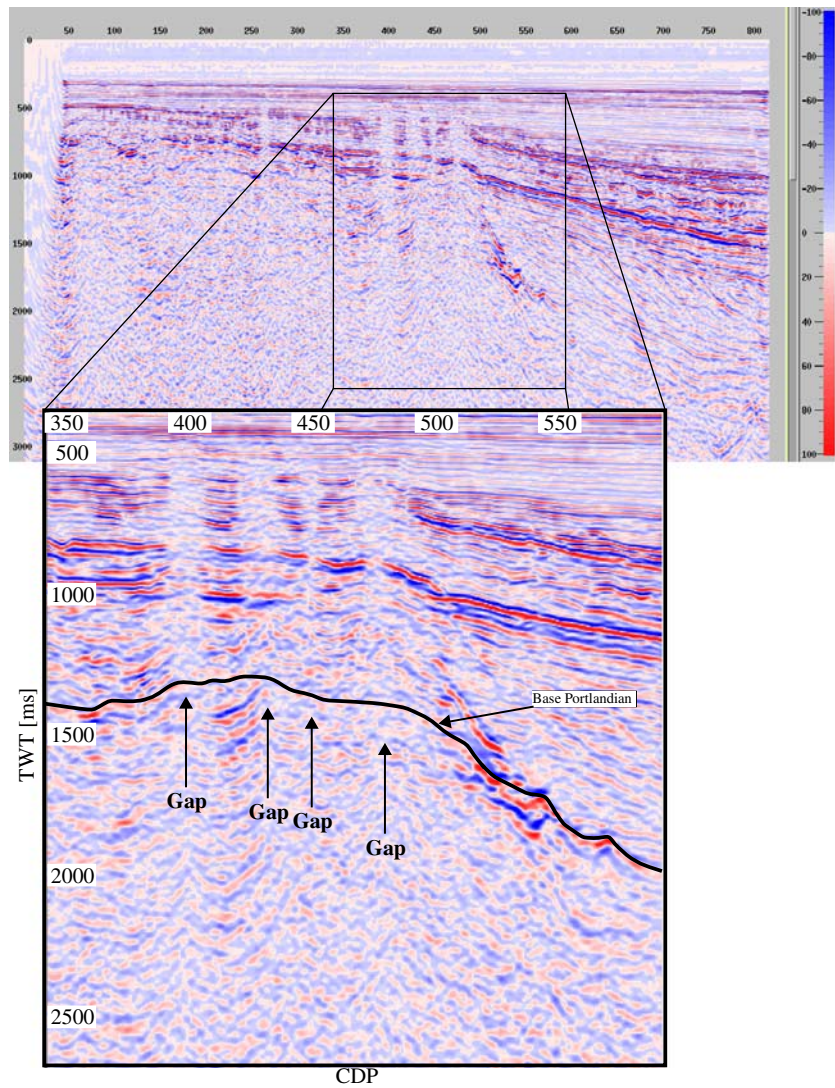
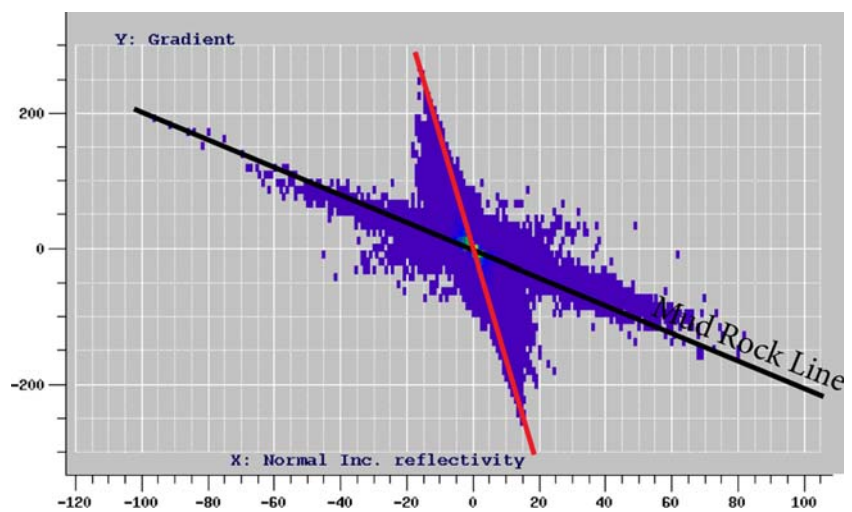


Fig. 15 Crossplot of Normal Incidence Reflectivity against AVO gradient for profile GEO1313. The *black line* represents the linear background trend (which is a typical one for clastic silicate rocks) and the *red line* the AVO anomalies over the complete profile, which are properly viewed as deviations from the background trend and may be related to hydrocarbons in the underground



cut by small faults, which might have favoured the leakage of hydrocarbons (Fig. 14). This possible leakage correlates to some extent with the distribution of

the gas chimneys on the sea floor (Fig. 2). Between CDPs 500 and 800, no chimneys were mapped on the seafloor and no more vertical structures can be recog-

nised in the deeper part of the Normal Incidence Reflectivity section (Fig. 14). Chimneys mainly occur along line GEO01313 between CDPs 250 and 500, and correlate with low-amplitude zones, indicating gas migration pathways in the subsurface above 1,000 ms. From Fig. 2 it can be derived that this is a 3D process, based on the gas chimney distribution south of profile GEO01313. At the moment we can only speculate whether the western onset of the chimneys simply correlates with the presence of the structural high beneath the more southerly lines or it is influenced by other tectonic factors.

In the southwestern part of profile GEO01313, between CDPs 50 and 250, the Upper Jurassic gas-bearing horizons have probably less gas leakage, due to more continuous layering of the overburden (Fig. 8). Again, a gas exchange with a shallower unit at 500 ms (CDP 500) is speculative. However, the Fluid Factor panel of line GEO01313 (Fig. 13) allows the interpretation that this shallow unit also contains gas, or at least residuals of percolated gas.

Finally, the AVO analyses do not provide any information about the depth of the hydrocarbon source. Estimates of the depth of the source rocks are solely based on the detailed analyses of available well-log information.

Summary

Amplitude versus offset analyses of CDP-gathers support an interpretation that gas chimneys in the Porcupine Basin are fed, or were fed, from deep-seated gas bearing horizons. The AVO analyses cannot assess the age, or the gas/oil/water content of these horizons. The existence of gas, or residuals of percolated gas, in the layers of Tertiary or Cretaceous age in two presented profiles can be inferred from the AVO analyses, especially in the Normal Incidence and Fluid Factor panels. The presence of diffuse amplitude zones, rising up from the hydrocarbon source layers beneath the mapped chimneys, supports the existence of vertical hydrocarbon pathways through the basin fill. Variations in the Fluid Factor and Normal Incidence panels are strong indicators for the presence of gas at approximately 1 s TWT. Along line GEO01313, the correlation of the sea floor gas chimneys with structural variations in the deeper geology is very strong. Reactivated fault systems bordering a basement high might favour the leakage of gas to the sea floor. A possible scenario for the genesis of these features, which is described by Rabaute et al. (2003), could clearly be approved using the results of the AVO analyses to

interpret the correlation of the migration of hydrocarbons in the deeper underground together with the existence of surface expressions of fluid expulsion like gas chimneys, mud volcanoes and pockmarks: hydrocarbons generated in the Middle Jurassic source rocks further south in the Porcupine Basin migrated up-dip northwards to the Connemara Oil Field. Here, they either entered Upper Jurassic or Cretaceous traps, or percolated along fault planes to shallower layers and escaped through more permeable Upper Cretaceous and Tertiary sandstones.

Finally, we would like to give acknowledgement to the EU for the funding of this study (EESD-ENV-99-1), to Prof. J.-P. Henriët the project coordinator as well as to our EU partners from the GEOMOUND consortium for their close working relationship. A special thanks goes to STATOIL for making the 3D data available which was the basis for the AVO analyses.

References

- Aki K, Richards PG (1979) Quantitative seismology. W.H. Freeman and Co, San Francisco
- Castagna JP (1997) Principles of AVO crossplotting. *Leading Edge* 16:337–342
- Castagna JP, Batzle ML, Eastwood RL (1985) Relationships between compressional-wave and shear-wave velocities in clastic silicate rocks, *Geophysics* 50(4):571–581
- Huvenne VAI, De Mol B, Henriët JP (2003) A 3D seismic study of the morphology and spatial distribution of buried coral banks in the Porcupine Basin, SW of Ireland. *Mar Geol* 198:5–25
- Moore JG, Shannon PM (1992) Palaeocene-Eocene deltaic sedimentation, Porcupine Basin, offshore Ireland—a sequence stratigraphic approach. *First Break* 10(12):461–469
- Naylor D, Shannon PM (1982) Geology of offshore Ireland and west Britain. Graham and Trotman, London, p 161
- Ostrander W, Gassaway GS (1983) The use of offset dependent reflectivity in exploration. *SEG Abstr* 1983(1):637–638
- Rabaute A, Van Rensbergen P, Colpaert A, Claeys M (2003) Gas chimneys from source to surface: imaging and modelling in the Connemara Field, Porcupine Basin, *Geophysical Research Abstracts*, vol 5, 13513, European Geophysical Society 2003
- Shuey RT (1985) A simplification of the Zoeppritz equations, *Geophysics* 50(4):609–614
- Smith GC, Gidlow PM (1987) Weighted stacking for rock property estimation and detection of gas. *Geophys Prospect* 35:993–1014
- Soubaras R (1996) Explicit 3-D migration using equiripple polynomial expansion and Laplacian synthesis. *Geophysics* 61(5):1386–1393
- Van Rooij D, De Mol B, Huvenne V, Ivanov M, Henriët JP (2003) Seismic evidence of current-controlled sedimentation in the Belgica mound province, upper Porcupine slope, southwest of Ireland. *Mar Geol* 195:31–53
- Ziegler PA (1982) Geological atlas of western and central Europe. Shell Internationale Petroleum Maatschappij BV, The Hague, p 130